



12-1991

s-Channel helicity conservation in the reaction ...

Ronald E. Majoras

Follow this and additional works at: https://trace.tennessee.edu/utk_gradthes

Recommended Citation

Majoras, Ronald E., "s-Channel helicity conservation in the reaction " Master's Thesis, University of Tennessee, 1991.

https://trace.tennessee.edu/utk_gradthes/12468

This Thesis is brought to you for free and open access by the Graduate School at TRACE: Tennessee Research and Creative Exchange. It has been accepted for inclusion in Masters Theses by an authorized administrator of TRACE: Tennessee Research and Creative Exchange. For more information, please contact trace@utk.edu.

To the Graduate Council:

I am submitting herewith a thesis written by Ronald E. Majoras entitled "s-Channel helicity conservation in the reaction" I have examined the final electronic copy of this thesis for form and content and recommend that it be accepted in partial fulfillment of the requirements for the degree of Master of Science, with a major in Physics.

George Condo, Major Professor

We have read this thesis and recommend its acceptance:

William Bugg, Tom Handler

Accepted for the Council:

Carolyn R. Hodges

Vice Provost and Dean of the Graduate School

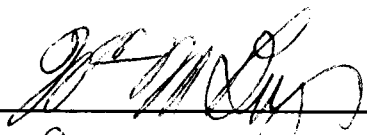
(Original signatures are on file with official student records.)

To the Graduate Council:


I am submitting herewith a thesis written by Ronald E. Majoras entitled "s-Channel Helicity Conservation in the Reaction $\gamma p \rightarrow \rho^0 n \pi^+$." I have examined the final copy of this thesis for form and content and recommend that it be accepted in partial fulfillment of the requirements for the degree of Master of Science, with a major in Physics.


George Condo, Major Professor

We have read this thesis
and recommend its acceptance:


Thomas Handke

Accepted for the Council:


Associate Vice Chancellor
and Dean Of The Graduate School

Statement Of Permission To Use

In presenting this thesis in partial fulfillment of the requirements for a Master's degree at The University of Tennessee, Knoxville, I agree that the Library shall make it available to borrowers under rules of the Library. Brief quotations from this thesis are allowable without special permission, provided that accurate acknowledgment of the source is made.

Permission for extensive quotation from or reproduction of this thesis may be granted by my major professor, or in his absence, by the Head of Interlibrary Services when, in the opinion of either, the proposed use of the material is for scholarly purposes. Any copying or use of the material in this thesis for financial gain shall not be allowed without my written permission.

Signature Ronald Majors

Date 21- November - 1991

s-Channel Helicity Conservation in
the Reaction $\gamma p \longrightarrow \rho^0 n \pi^+$

A Thesis

Presented for the

Master Of Science

Degree

The University of Tennessee, Knoxville

Ronald E. Majoras

December 1991

DEDICATION

This thesis is dedicated to my parents who got me started and to Traci who got me to finish.

ACKNOWLEDGMENTS

I would like to thank my major professor, George Condo, for all of his help whether it be suggestions, comments, or criticisms. I would like to thank my other committee members, William Bugg and Tom Handler for their help. I would like to thank Joe Hargis for his assistance with the computer-related aspects of this thesis. My family deserves a great deal of credit for their help and encouragement. Most of all, I would like to thank my wife, Traci. I would never have finished without her help and encouragement.

ABSTRACT

This research isolated the reaction $\gamma p \rightarrow N^{*+} \rho^0$, at $|t'_{\gamma\rho}| < 0.15(\text{GeV}/c)^2$, with the N^{*+} decaying into $n\pi^+$. The decay-angular distributions and Breit-Wigner resonance distribution for this reaction were examined. Comparisons were made with a similar type reaction, $\gamma p \rightarrow \rho^0 p \pi^+ \pi^-$.

It was determined that the s-channel helicity of the ρ^0 is approximately conserved in this reaction and that the $\pi^+ \pi^-$ mass distribution is skewed in a manner that is consistent with inelastic ρ^0 photoproduction.

Table Of Contents

CHAPTER	PAGE
1. INTRODUCTION.....	1
2. THE EXPERIMENT.....	2
THE PHOTON BEAM LINE.....	2
THE BUBBLE CHAMBER.....	4
PROPORTIONAL WIRE AND CERENKOV COUNTERS.....	5
THE LEAD GLASS WALL.....	6
3. DATA PROCESSING.....	8
EVENT SELECTION BY SCANNING.....	8
EVENT SELECTION BY STATISTICAL MEANS.....	9
4. DATA ANALYSIS.....	12
ρ^0 PHOTOPRODUCTION.....	12
s-CHANNEL HELICITY CONSERVATION.....	14
5. CONCLUSIONS.....	16
REFERENCES.....	17
APPENDIX.....	19
VITA.....	26

LIST OF FIGURES

FIGURE		PAGE
Figure 4.1.	This is the mass distribution for all possible $\pi^+\pi^-$ combinations.....	20
Figure 4.2	This histogram is the $\pi^+\pi^-$ mass distribution after the cut $ t'_{\gamma\rho} < 0.15(\text{GeV}/c)^2$	21
Figure 4.3	This histogram is the $\pi^+\pi^-$ mass distribution fitted to a Breit-Wigner distribution. The solid curve represents the fit.....	22
Figure 4.4	This histogram is the recoil mass ($n\pi^+$) distribution. The cuts $ t'_{\gamma\rho} < 0.15 (\text{GeV}/c)^2$ and $550 \leq M_{\pi\pi} \leq 900 \text{ MeV}/c^2$ were both applied to the data in order to obtain this plot.....	23
Figure 4.5	(a) $\cos\theta$ angular distribution and (b) $\cos\theta$ angular distribution with fit.....	24
Figure 4.6	(a) ψ angular distribution and (b) ψ angular distribution with fit.....	25

CHAPTER 1 Introduction

This thesis is based upon data taken from the SLAC experiment BC72/73 which was performed at the SLAC Hybrid Facility in the years 1980-1982. The primary purpose of this experiment was to study photoproduction of charmed particles. Because of its large size, many auxiliary problems have proved to be amenable to study.

Chapter 2 covers the experimental apparatus of BC72/73. Chapter 3 covers the preliminary data selection. Chapter 4 covers data analysis and results. Chapter 5 presents the conclusions.

CHAPTER 2 The Experiment

There were four essential components of this experiment: a Compton backscattered photon beam and its associated detectors, the SLAC 1 meter bubble chamber together with its optics system, Cerenkov and proportional wire counters (PWCs), and a lead glass calorimeter. This chapter will describe these components in greater detail.

2.1 The Photon Beam Line

The photon beam was produced by backscattering 4.7 eV photons off a 30 GeV electron beam. The electron beam, consisting of groups of electrons emitted in bursts of approximately 100 ns with a peak current of 50 mA, was fed into the experimental beamline from the SLAC LINAC. Using a series of dipole and quadrupole magnets, this electron beam was focused into the electron-laser interaction region.

Inside the interaction region, ultraviolet photons produced by a Neodymium doped Yttrium Aluminum Garnet (Nd:YAG) laser, interacted with the electron beam at an

angle of 2 mrad. This interaction caused Compton scattering and the backscattered photons became the photon beam for the experiment.

This photon beam has an energy of approximately 19.5 GeV with a spread of about 1.0 GeV. The beam is also highly plane polarized. These three factors are the important beam parameters in photoproduction experiments.

Downstream, at a distance of 150 m from the electron-laser interaction region, is the apparatus used for determining the photon beam characteristics. First in line is the Quadrant Detector. It has the dual role of obtaining the photon beam kinematic parameters and steering the beam with a system of mirrors and magnets.

Located immediately behind the Quadrant Detector is the Pair-Spectrometer. As the name suggests, the Pair-Spectrometer detects e^+e^- pairs. The Pair-Spectrometer contains a radiator foil made of aluminum or copper that converts a fraction of the photon beam into e^+e^- pairs. These pairs are deflected by the spectrometer's analyzer magnet which allows the determination of the momentum and energy of the photon beam. The number of pairs that are produced determines the beam intensity. These measured photon beam parameters are the ones seen by the target.

2.2 The Bubble Chamber

The SLAC 1 meter bubble chamber simultaneously provides a liquid hydrogen target and detector for the photon beam. The hydrogen is the source of protons for the photon-proton interaction being studied.

The general operation of the bubble chamber involves keeping the liquid at pressures between five and twenty atmospheres and then suddenly expanding it with a piston to achieve superheating. This superheating causes bubbles to occur along tracks of charged particles. These tracks are photographed by an array of cameras using flash illumination that gives a "pictorial" history of the charged particle. The bubble chamber is then decompressed. An advantage of this technique is that the compression-decompression cycle can be triggered to look at only what is deemed to be relevant.

The bubble chamber was surrounded by a large magnet that was operated at 26 KG for fifty percent of the experimental run and 18.5 KG for the other fifty percent of the run. This magnet produced a magnetic field in the Z direction that

caused the bending of a charged particle's path in the X-Y plane of the bubble chamber.

In this experiment three cameras and a special high resolution camera were used to achieve a stereoscopic view of the tracks formed by the bubbles. The high resolution camera was capable of a resolution of approximately 55 micrometers over a depth of 6 mm above and below the interaction plane. A momentum measurement of the particle can be made from the pictures taken of the particle's path through the bubble chamber. With these data it is possible to identify particles up to a maximum momentum of approximately 1.4 GeV.¹

2.3 Proportional Wire and Cerenkov Counters

In this experiment there were three sets of proportional wire counters situated behind the bubble chamber. Each of these PWCs had three wire planes: a horizontal plane, a vertical plane, and a diagonal plane. If the horizontal plane detects a charged particle, an attempt is made to correlate a bubble chamber track with the hit. If the hit was caused by the track in the bubble chamber, the event is

used to trigger the compression-decompression cycle of the bubble chamber. In addition, this information leads to increased resolution of the track's momentum.

As mentioned earlier the bubble chamber and its optical system is fine for identifying particles with momenta up to 1.4 GeV. It is the function of the Cerenkov Counters to help identify particles with momenta that exceeds 1.4 GeV. Essentially a Cerenkov counter can distinguish between two relativistic particles that have the same momentum but different masses. There were two Cerenkov Counters positioned behind the PWCs. The first counter contained Freon and the second counter contained nitrogen. By using two counters with different gases, it is possible to set different threshold values for the particles.²

2.4 The Lead Glass Wall

The lead glass wall is a calorimeter which is situated 6.4 meters from the bubble chamber. As the name suggests, the interaction region of the lead glass wall is mostly composed of lead. Its major goal is to identify π^0 's that were produced. The first component of this apparatus is the

filter hodoscope which distinguishes between electron initiated and photon initiated showers. Directly behind the hodoscope sits a lead shield that converts the photons into e^+e^- pairs. This is followed by an active converter of lead glass which distinguishes between hadronic and electromagnetic showers. Photomultiplier tubes in this section observe the electromagnetic showers. Behind this section are finger hodoscopes that determine the position of showers. The last elements are the lead glass blocks which determine the shower energy.

As stated, it is the purpose of this detector to detect π^0 's. The π^0 decays into two photons 99% of the time. These photons enter the Lead Glass Wall and generate electromagnetic showers. These showers generate Cerenkov light that is detected by photomultiplier tubes. The amount of light observed is proportional to the energy of the incoming photon.

CHAPTER 3 Data Processing

The particular reaction that is of interest in this thesis is $\gamma p \rightarrow n \rho^0 \pi^+$. During the experiment, there were two gigabytes of data collected and stored on twelve data survey tapes.² From this massive amount of data, the data relevant to this reaction was selected. It is the purpose of this section to describe this selection process.

3.1 Event Selection by Scanning

Recall from section 2.2 that the bubble chamber was surrounded by cameras that would take pictures of tracks left by charged particles passing through the superheated hydrogen. The selection and categorization of events starts with the scanning of the bubble chamber film. If the picture contained an hadronic event then the prong count, vertex position, number of kinks in the charged tracks, and the number of Dalitz pairs was recorded for that event. This information is encoded on the data summary tape for later

analysis. There were over 300,000 hadronic events measured for this experiment.

The only events that were of interest for this thesis were three prong events, a prong being the track a charged particle leaves in the bubble chamber. Therefore, the next data cut involved eliminating all the events that had more than three prongs. This reduced the number of events for analysis to 30,638.

3.2 Event Selection by Statistical Means

The $\gamma p \rightarrow n\pi^+\pi^+\pi^-$ events were determined by using those three prong events that have a three-constraint (3C) kinematic fit to other hypothesis. A three constraint fit means that each track has been measured and no particle is left unidentified. Additionally, the curvature, momentum, and the azimuthal angle (the three constraints) have been successfully determined for each event. Since it is not possible to measure a neutron track, the 3C fit was used to exclude the events that were successfully fitted. Two algorithms, TVGP and SQUAW³, attempt to make these fits.

The TVGP algorithm attempts to reconstruct each event that was seen on film. It calculates the 3-dimensional momentum vectors associated with each event and it predicts the ionization loss for each particle. Since ionization loss is related to the velocity of the particle, this information can be used in helping to identify the particle.⁴ With this information the TVGP algorithm determines every conceivable interpretation of the track.

Next, the SQUAW algorithm attempts to make a kinematic fit to these hypothesized tracks by invoking the conservation of momentum, energy, and charge laws for the particles involved. This is done by assigning a particle (p, π^+ , π^- , K^+ , etc.) to each observed track in the event. The algorithm then calculates the χ^2 value for each possible fit. The fit with the best χ^2 determines the event type. If the probability of the fit as determined by the χ^2 was greater than 0.1% then the event was rejected.

From this sample, any event that contained a track that could be interpreted as a proton based on ionization, curvature, or Cerenkov data was rejected. Any event that was associated with one or more photons in the lead-glass wall was rejected. Finally, if the initial gamma energy, E_γ , was not between 15.0 GeV and 22.0 GeV, the event was eliminated

from the sample. This series of cuts leaves approximately 8,000 events for the physics analysis.

CHAPTER 4 Data Analysis

This section will describe the process of selecting the $\rho^0(770)$'s. The process of testing for s-channel helicity conservation along with the results of the test will be presented as well. Comparisons will be made with the paper by K. Abe et al⁵ (to be referred to as the Brau-Shimony paper) that describes the four prong reaction $\gamma p \longrightarrow \rho^0 p \pi^+ \pi^-$.

4.1 ρ^0 Photoproduction

Since the ρ^0 decays into a $\pi^+ \pi^-$ combination, only events that contain this dipion combination are examined. Figure 4.1 shows the $\pi^+ \pi^-$ distribution for these 7,738 events.*

Next a cut was made based on the value of t' which is the square of the four-momentum transferred from the photon to the ρ^0 . This results in restricting the events to only those that have a $|t'_{\gamma\rho}| = |t - t_{\min}| < 0.15(\text{GeV}/c)^2$. Figure 4.2 is the mass spectrum for these 1,186 events. The ρ^0 signal can be observed

* All figures may be found in the Appendix.

in this spectrum. It is clear that the mass distribution is skewed.

This spectrum is fitted with a curve representing a Breit-Wigner distribution for ρ production. The Breit-Wigner fit is given by the expression

$$\frac{d\sigma}{dm} = \frac{m}{q} \frac{m_\rho \Gamma_\rho}{(m_\rho^2 - m^2)^2 + m_\rho^2 \Gamma_\rho^2} .$$

In this equation, q is the pion momentum in the center of mass of the dipion system, m_ρ is the mass of the ρ , and Γ_ρ is width of the ρ . The fit was made by varying m_ρ and Γ_ρ , and subjecting the results to a best χ^2 fit. The results are plotted in Fig. 4.3. with $m_\rho = 708 \pm 5$ Mev/c² and $\Gamma_\rho = 157 \pm 14$ Mev/c².

In the Brau-Shimony paper, the reaction $\gamma p \rightarrow 2\pi^+ 2\pi^- p$ is examined. They also plot the spectrum for the dipion system with the cuts $|t'| < 1.0$ GeV/c² and momentum > 16 GeV/c. Their spectrum is quite similar to ours in that it displays the usual skewing observed in diffractive ρ^0 photoproduction with a central mass value somewhat less than 750 MeV.

Figure 4.4 is a plot of $n\pi^+$ mass distribution for the pions opposite the pions in the dipion system. For this plot, an additional mass cut was made requiring that only those pions that were opposite the dipion system $550 \leq M_{\pi\pi} \leq 900$ MeV/c² be selected. This plot compares favorably with

Brau-Shimony plot of the recoil mass distribution for the reaction $\gamma p \rightarrow \rho^0(p\pi^+\pi^-)$, with the recoil mass for this reaction consisting of the particles in parentheses.

4.2 s-Channel Helicity Conservation (SCHC)

If s-channel helicity is conserved then the ρ^0 will have helicity ± 1 and

$$W(\cos\theta, \psi) = \left[\frac{3}{8\pi}\sin^2\theta\right](1 + P_\gamma \cos 2\psi).$$

In this equation θ represents the angle between the π^+ in the ρ rest frame relative to the ρ direction of flight. The angle ψ represents the difference between the azimuthal angles in the ρ rest frame and in the center-of-mass frame. P_γ is the degree of photon polarization.

Figure 4.5a is a plot of $\cos\theta$ and Fig. 4.6a is a plot of ψ . Both plots are defined by the earlier cuts $|t'| < 0.15$ GeV/c² and $550 \leq M_{\pi\pi} \leq 900$ MeV/c². Figures 4.5b and 4.6b are the same distributions only they have been fitted (solid curve) to the appropriate distributions.

The ψ distribution fit resulted in $P_\gamma = 0.42 \pm 0.04$. The Brau-Shimony paper showed that their distribution was

reasonably consistent with the expected value, $P_\gamma=0.52$, if they subtracted off a 20% uniform background contribution. This background contribution was not estimated for this thesis and can account for the differences in the values for P_γ .

The angular distribution in Fig 4.5a was fit to $\cos^2\theta$. The fit to a $\cos^2\theta$ distribution had a χ^2 per degree of freedom of 0.76 without a background contribution.

CHAPTER 5 Conclusions

In this thesis we have isolated the reaction $\gamma p \rightarrow N^{*+} \rho^0$, at $|t'_{\gamma\rho}| < 0.15(\text{GeV}/c)^2$, with the N^{*+} decaying to $n\pi^+$. By studying the angular decay distributions we determined that the s-channel helicity of the ρ^0 is approximately conserved in this reaction. In other words this is an example of inelastic ρ^0 photoproduction. A similar work initiated by Brau and Shimony studied a similar reaction but in their case the N^* decayed to $\Delta^{++}\pi^-$. They also concluded that s channel helicity conservation was present in the inelastic ρ^0 photoproduction. In our experiment there is no clearly defined peak associated with any particular N^* production. This situation is similar to other N^* "production-type" experiments whether induced by pion-proton reactions or the Brau-Shimony study.

REFERENCES

¹Proton and Pion Identification at Low Momenta, BC72/73 Note No.357, G.Yost, Nov.6,1985.

²E.McCrory, Ph.D. Thesis, Duke University, 1986.

³Dahl, O.I., T. B. Day, and F.T. Solmitz, Group A Programming Note P-126 (1968), University Of California, Lawrence Berkley Laboratory.

⁴E.McCrory, Ph.D. Thesis, Duke University, 1986.

⁵K.Abe et al.Phys. Rev. D 32, 2288 (1985).

APPENDIX

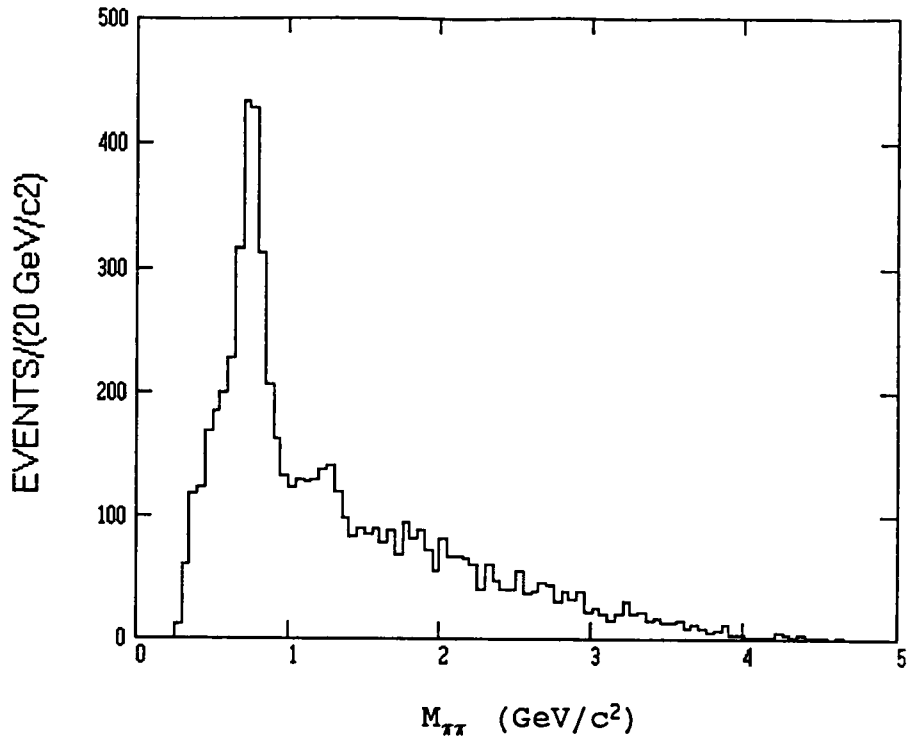


Figure 4.1. This is the mass distribution for all possible $\pi^+\pi^-$ combinations.

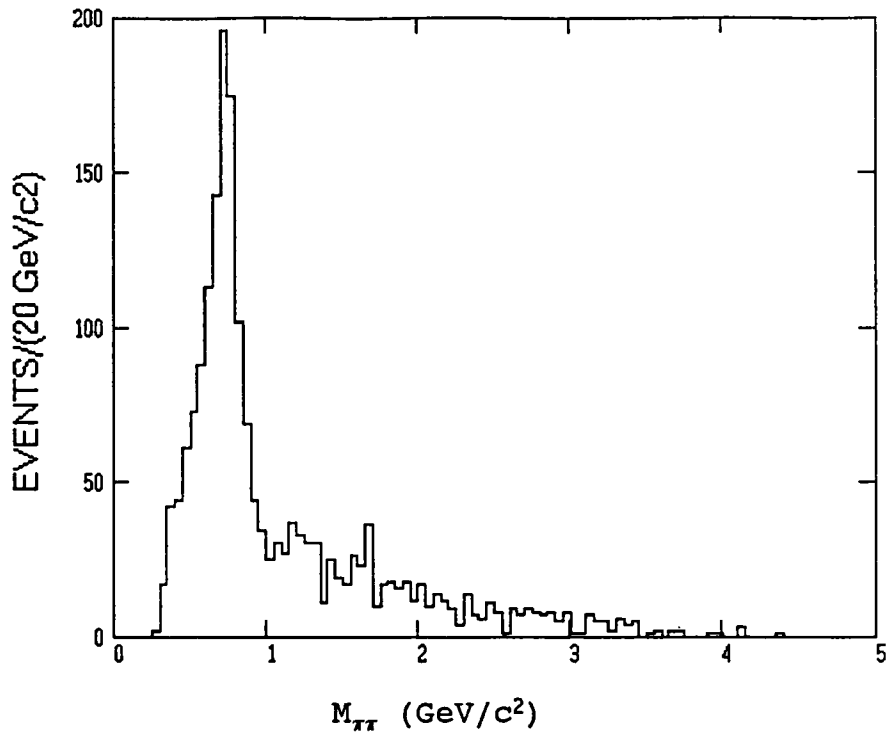


Figure 4.2 This histogram is the $\pi^+\pi^-$ mass distribution after the cut $|t'_{\gamma 0}| < 0.15(\text{GeV}/c)^2$

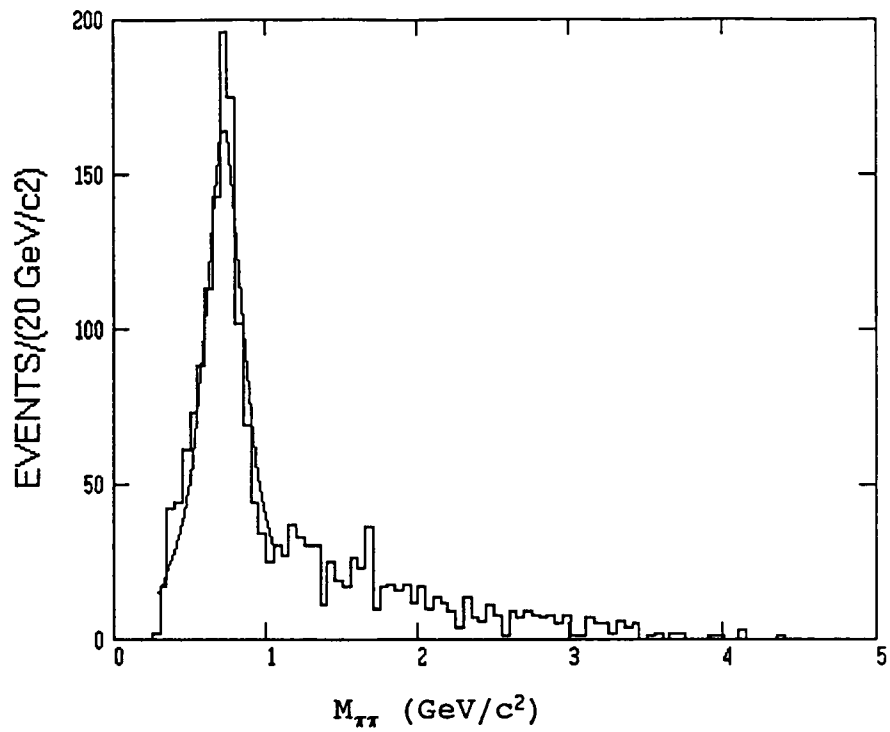


Figure 4.3 This histogram is the $\pi^+\pi^-$ mass distribution fitted to a Breit-Wigner distribution. The solid curve represents the fit.

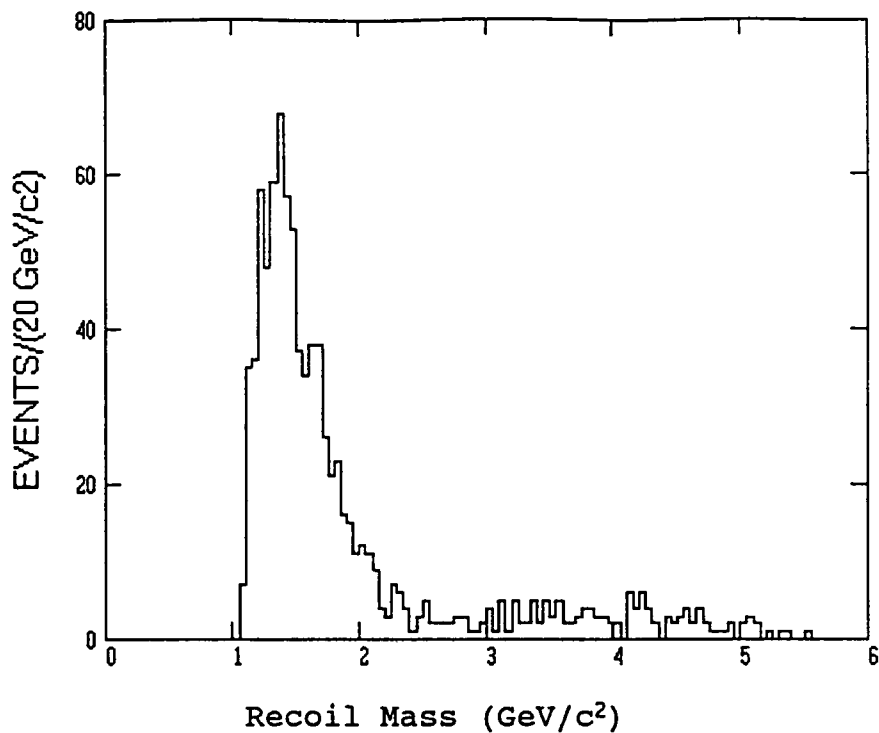


Figure 4.4 This histogram is the recoil mass ($n\pi^+$) distribution. The cuts $|t'_{\gamma p}| < 0.15 \text{ (GeV/c)}^2$ and $550 \leq M_{\pi\pi} \leq 900 \text{ MeV/c}^2$ were both applied to the data in order to obtain this plot.

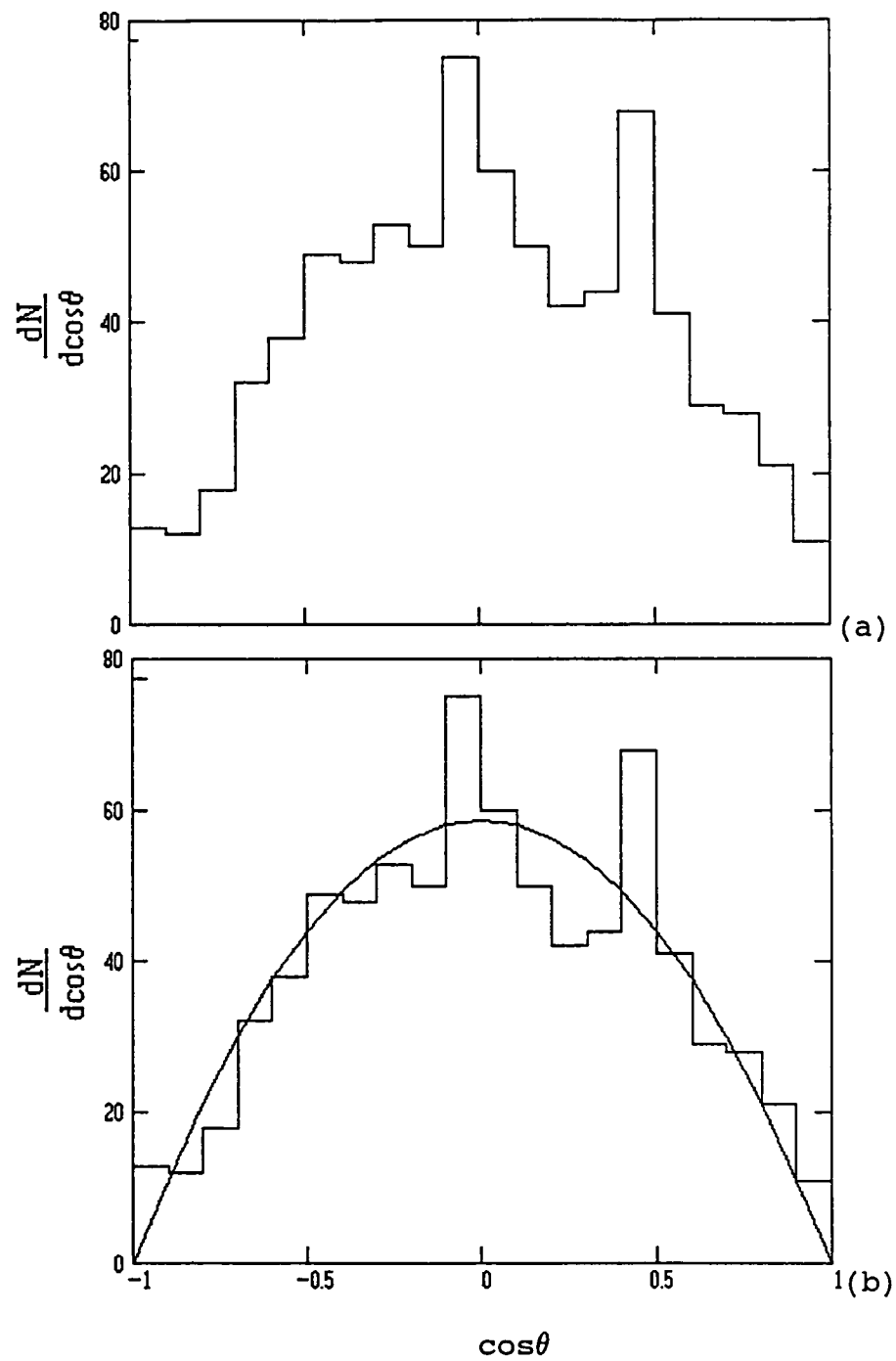


Figure 4.5 (a) $\cos\theta$ angular distribution and (b) $\cos\theta$ angular distribution with fit.

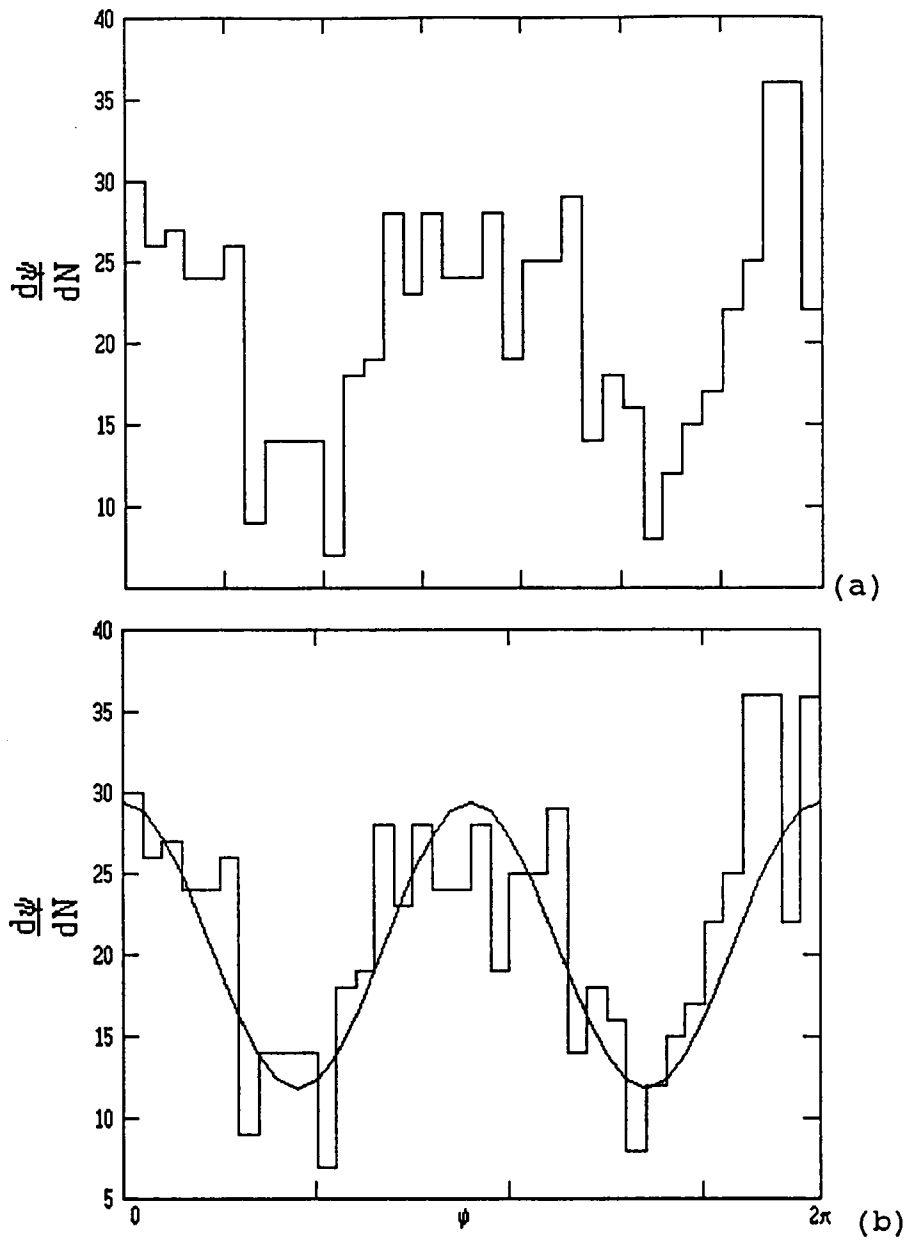


Figure 4.6 (a) ψ angular distribution and (b) ψ angular distribution with fit.

VITA

Ronald E. Majoras was born in Elyria, Ohio on April 8, 1960. He currently lives and works in Knoxville, Tennessee.